Additive Manufacturing 97 (2025) 104609

Contents lists available at ScienceDirect

Additive Manufacturing

journal homepage: www.elsevier.com/locate/addma

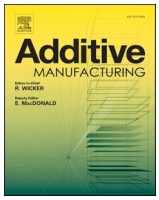

Drying-oriented resolution optimization for multi-material additive manufacturing: A case study on coffee-ring effect

Ningji Wei [a,*], Hur-E-Jannat Moni [b], Qiang Jiang [c], Yanliang Zhang [c], Minxiang Zeng [b,*]

[a] Department of Industrial, Manufacturing and Systems Engineering, Texas Tech University, Lubbock, TX 79409, USA
[b] Department of Chemical Engineering, Texas Tech University, Lubbock, TX 79409, USA
[c] Department of Aerospace and Mechanical Engineering, University of Notre Dame, Notre Dame, IN 46556, USA

ARTICLE INFO

Keywords:
Coffee-ring effect
Solution-based processing
Aerosol-jet printing
Manufacturing optimization

ABSTRACT

While ink-based printing methods have been explored for creating novel materials and structures, the underlying impact of ink drying on printed materials, especially in the context of multi-axis, multi-material additive manufacturing (AM), is not well understood. Here, we investigate how different drying shapes affect the printing performance (e.g., composition, printing offset) using additive manufacturing of gradient materials as a case study. Different drying scenarios of coffee-ring effects are identified using shape functions, and their resulting influences on the uniformity and control of compositional gradients are showcased. While ideal deposition aims for continuously gradient materials, we observe that uneven ink drying poses a non-negligible effect on the composition of printed gradients. This has led to a required minimal offset (i.e. printing resolution in the AM process) for maintaining deposition gradient stability. This study presents a mathematical model to explain how the cross-sectional shape of a droplet, printing gradient resolution, and material gradient stability are related, predicting whether a uniform gradient will form based on the droplet's shape function after drying. Additionally, it introduces a drying-focused resolution optimization framework, capable of handling various droplet shapes, regardless of symmetry or concavity, to estimate the minimum printing resolution required for multi-material combinatorial fabrication.

1. Introduction

Ink-based printing, as a popular additive manufacturing approach, involves the deposition and subsequent drying of dispersions or slurries for rapid prototyping of functional materials and devices [1–3]. This technique has attracted tremendous research interest as this process is compatible with a wide range of materials [4]. In contrast to relatively mature single-material printing, compositional control via multi-material 3D printing remains at its early stage as the vastly different properties of dissimilar materials make it difficult to deposit different materials within one printing system precisely under reasonable printing resolution. In the effort to address this challenge, various deposition mechanisms of multi-material printing (MMP) have been explored, including extrusion printing [5], inkjet printing (IJP) [6,7], and aerosol jet printing (AJP) [8–11]. These findings have led to progress in several engineering areas, including combinatorial material library [12] and functionally graded materials [13–15]. For example, AJP handles multiple materials by switching inks, which were independently atomized via ultrasonic or pneumatic methods and then focused using a sheath gas through a nozzle. This allows precise deposition of complex patterns for printed electronics [16–18] and the creation of multi-material structures with varying properties [12]. Despite these successes, it remains unclear regarding the practical impact of ink spreading/drying on printing resolution and the resulting structures of multi-material samples. Filling this knowledge gap will benefit the design and precise manufacturing of next-generation complex materials with controlled compositions.

There are several factors dictating the accuracy of printing. For ink-based printing (e.g., inkjet printing, aerosol jet printing, solvent-based extrusion printing), the way ink droplets interact with substrate surface during drying process plays a crucial role in printed structure (e.g., shape fidelity for single material deposition; composition fidelity for multi-material deposition). A particularly common and arguably undesirable outcome of this process is the "coffee-ring effect," observed during the drying phase of the ink [15]. This phenomenon emerges due to the uneven evaporation of the solvent within the droplet: evaporation

* Corresponding authors.
E-mail addresses: ningji.wei@ttu.edu (N. Wei), minzeng@ttu.edu (M. Zeng).

https://doi.org/10.1016/j.addma.2024.104609
Received 24 August 2024; Received in revised form 11 December 2024; Accepted 13 December 2024
Available online 14 December 2024

tends to occur more rapidly around the droplet's periphery (Fig. 1A), and this uneven drying leads to an outward convection current carrying along dispersed ink nanomaterials. As a result, these materials accumulate at the edges of the droplet, often leaving the center nearly empty of any material. The uneven deposition of materials often causes deposition variation for ink-based printing, whereas the coffee ring effect can be useful sometimes for certain applications such as transparent electronics and aligning 1D nanomaterial for enhanced electrical property [19]. The formation of coffee-ring effect can be strongly influenced by various factors including temperature [20], particle surface charge (zeta potential) [21,22], particle size [23], concentration [24], leading to different shapes of deposited materials. While several reports have studied the mitigation of the coffee-ring effect experimentally [25–29], a comprehensive understanding of how it affects the printing variability (e.g., compositional accuracy) is missing, consequently limiting the development of an optimization strategy for ink-based printing. Experiments with parametric optimization have been developed in several single-material additive manufacturing processes [30–32] to improve their printing resolutions and material performances. However, for MMP, such optimization techniques are still notably absent as the underlying relationship between printing resolution and compositional accuracy remains evasive.

This paper proposes a drying-oriented resolution optimization (DORO) approach along with a new analysis framework that quantifies the relationship between the cross-section droplet shape, the printing resolution, and the gradient stability. This framework reveals the impact of the coffee-ring effects on printed functionally graded materials (FGMs), explains the well-observed compositional gradient stability associated with concave-shaped droplets, and provides tools for optimizing printing resolution while maintaining multi-material stability. While the mitigation of coffee-ring effect is considered, it is not the central focus of this work. Instead, this work emphasizes the impact of coffee-ring drying on printing performance based on the dried droplet shapes, which can vary depending on other factors such as drying temperature, concentration of materials, solvents, etc. Fig. 1B demonstrated a few classic scenarios of deposited materials after droplet drying, where the uneven distribution of material is caused by different degrees of coffee-ring effect. The severity of this effect influences whether the deposition forms a 'ring shape', with material concentrating at the droplet edges, or a 'hill shape', with material accumulating at the center. To better visualize this uneven distribution, a color coding is used: darker shades indicate higher material content, while lighter shades are for less material. Red and blue represent different materials in multi-material printing to differentiate their distribution patterns. To quantify this effect on MMP, we propose a shape function of dried droplets and showcase its influence on the uniformity and stability of compositional gradients mathematically (workflow as shown in Fig. 1C). Additionally, we compared the composition gradient stability of printed materials with our DORO model, showing a clear, consistent trend for printing resolution prediction. A brief literature survey on the current studies is listed in Table 1 to emphasize the unique contribution of this work.

2. Material and methods

2.1. Materials

The materials used in this study include silver nanoparticle ink (Ag, 30 wt% dispersion, Sigma-Aldrich), kaolinite (Sigma-Aldrich), halloysite nanoclay (Sigma-Aldrich), ethylene glycol (EG, ≥99.0 %, VWR Chemicals), and isopropyl alcohol (IPA, ≥99 %, J.T.Baker®). Bismuth telluride (Bi_2Te_3) was synthesized via previously reported method [39].

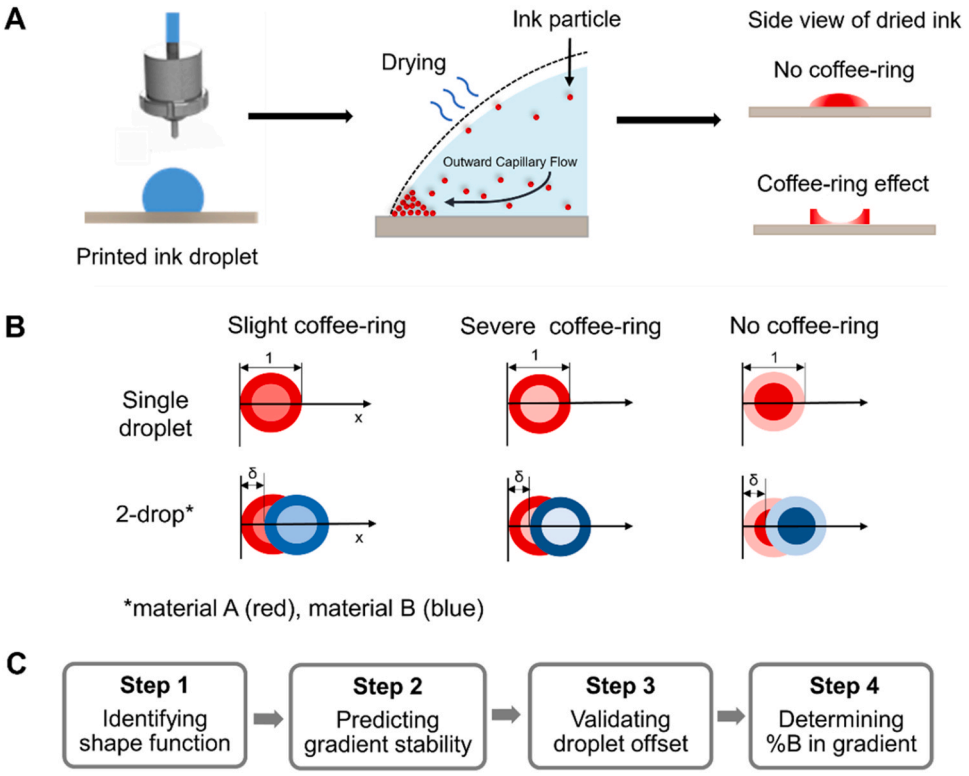

Fig. 1. Overview of the coffee-ring effect on material deposition. A) Schematics of ink drying process in additive manufacturing (single droplet scenario). B) Examples of dried droplets under different drying effects such as slight, severe, and no coffee-ring effects. Droplets can be 'ring-shaped' with material concentrated at the edges or 'hill-shaped' with material concentrated at the center. Darker colors indicate higher material content, while lighter colors show lower content. Red and blue represent different materials. Each droplet's diameter is normalized assuming consistent deposition (drying effect of deposited ink line is similarly applicable though coffee ring effect of ink lines will be one dimensional). C) Workflow of drying-oriented resolution optimization (DORO) approach.

Table 1
A brief summary of current studies on the drying process in additive manufacturing, suggesting a knowledge gap on composition effect from drying phenomena. PEDOT: Poly(3,4-ethylenedioxythiophene); PSS: Poly(styrenesulfonate); PVDF: Poly(vinylidene fluoride).

Printing Method	Materials	Contributions to drying process in additive manufacturing	Ref.
IJP	PEDOT:PSS	Print uniform lines with controlled coffee ring effects and improve the precision of electronic devices.	[33]
IJP	Organic semiconductors	Improve the film homogeneity and uniformity in organic light emitting devices (OLEDs) by controlling the polarity and viscosity of inks to mitigate contact line receding and coffee ring effect.	[30]
IJP	Graphene	Mitigate the coffee-ring effect using porous cellulose nanopaper instead of non-porous glass substrates.	[34]
AJP	Carbon nanotubes	Improve uniformity and stability in carbon nanotube thin-film transistors by optimizing the temperature and aerosol dynamics.	[35]
AJP	Carbon nanotubes	Optimize the concentration of sodium dodecyl sulfate in the ink to achieve dense film depositions to control the coffee-ring effect.	[36]
AJP	Ag	Propose a machine learning framework to optimize printing parameters to improve the quality and precision of printed electronic lines.	[37]
Microplotter Printing	PVDF	Use high-viscosity ink to reduce the coffee-ring effect to achieve uniform deposition of materials and to improve the quality of the printed electronic devices.	[38]
AJP	Ag-Bi_2Te_3 (gradient materials)	Optimization framework to predict minimal printing offset for stable compositional gradients from drying shape of droplets.	This work

Specifically, $Bi(NO_3)_3{\cdot}5\,H_2O$ (18 mmol), Na_2TeO_3 (27 mmol), NaOH (5 g), and polyvinylpyrrolidone (40,000 g mol^{-1}, 2.4 g) are added to a 200 mL ethylene glycol. The mixture was heated under reflux conditions overnight to ensure reaction completeness. Bi_2Te_3 particles are separated by centrifugation at 5000 rpm and subsequently washed 3 times with ethanol to remove residuals.

2.2. Ink formulation

In a standard aqueous ink formulation, Bi_2Te_3 were dispersed in a solvent mixture of water and EG. Here, EG acted as a co-solvent, enhancing ink stability and printability. To mitigate foam during ultrasonic atomization, a minor quantity of IPA was incorporated as an antifoaming agent. To prevent particle aggregation and ensure homogeneous dispersion, the inks underwent sonication for 15 minutes using a Hilsonic bath sonicator at 300 W. The nanomaterial concentration was confirmed using the dry weight method.

2.3. Printing and characterization

The ink-based multi-material printing is based on a custom-built aerosol jet printer. The printer's motion control interface manages its X, Y, and Z axes, enabling tracking of position and velocity during both targeted movements and jogging operations. Concurrently, the printer adjusts the flow rates of two aerosol inks based on the stage's location, yielding gradient material films. After initial ink priming through 30 minutes of sonication, the inks were atomized using ultrasonication and then carried to the printhead using nitrogen gas. To narrow the aerosolized ink stream and enhance printing precision, a sheath flow technique is employed. For the gradient structure of Ag-Bi_2Te_3 films, the glass substrate was first treated under air plasma. Subsequently, gradient material layers were applied. During the printing of these gradient layers, the ink ratio of Ag ink to Bi_2Te_3 ink was gradually adjusted from 1:0–0:1. A heated stage (Thermo Scientific CERAMIC+) is applied to speed up the evaporation of ink solvents. All substrates were positioned at the center of the hotplate to maintain a minimal temperature difference. The optical profilometer (Profilm3D, KLA) was used to map the thickness and surface morphology of the deposited materials. It operates by capturing high-resolution 3D surface images through white light interferometry, and this provides measurement of surface height variations with high vertical resolution. This non-contact technique is ideal for quantifying the shape functions of printed lines, which will be used to evaluate surface morphology and thickness uniformity across the sample. For temperature control, a heating platen was applied with a stage size of 7.25 in x 7.25 in (Max temperature capacity: 540°C). Additional parameters used in the multi-material AJP printing are summarized in Table 2.

2.4. Modelling of 2-drop

To quantify the effect of coffee-ring drying patterns on printing uncertainty and gradient stability, we first consider a simple 2-drop scenario (multiple drop situation is also considered and can be found in the next section). This section introduces the analytical tools for investigating the coffee-ring effects in a 2-drop setting. We use a shape function $\sigma : R \to [0, \infty]$ to represent the cross-section shape of a droplet with a normalized unit width and have the following assumptions.

Assumptions:

- Shape function σ is second-order differentiable almost everywhere (a.e.) and satisfies $\sigma(x) > 0$ for all $x \in (0,1)$ and $x = 0$ otherwise, where non-zero values of σ indicate actual material deposition.
- In the same printing session, every droplet is represented by $\sigma(x-\delta)$ for some offset $\delta \in (0,1)$, where the offset is the minimal spacing between two adjacent depositions of material-varying inks. A smaller offset indicates a higher printing resolution.
- Shape functions are additive (i.e., the printing thickness is additive): for two droplets $\sigma(x)$ and $\sigma(x-\delta)$, the composed material has the shape function $\sigma(x) + \sigma(x-\delta)$.

For a given shape function $\sigma(x)$, we can further define the (2-drop) composition ratio function $r(\cdot)$ for two droplets with offsets 0 and δ as follows. The composition ratio relates to the experimentally measured volume fraction of secondary materials in functionally graded materials (FGMs).

Volume Fraction of2nd Material :

$$r(x) = \frac{\sigma(x-\delta)}{\sigma(x) + \sigma(x-\delta)};\ x \in [0 \quad , 1+\delta] \tag{1}$$

This represents an MMP scenario where both drops have distinct printing materials. Thus, the value $r(x)$ indicates the composition ratio of the second material at location x. In the ideal case, this value increases gradually from zero to one, forming a smooth transition in material composition. However, the coffee-ring effects can compromise such

Table 2
Summary of parameters of combinatorial multi-material AJP printing.

Parameters	Values
Nozzle nominal I.D.	22 G
Ink flow rate (sccm)	0–28
Sheath gas flow rate (sccm)	20–160
Platen temperature (°C)	85
Print speed (mm/s)	4

desired properties for small offsets, causing structural instability in the resulting composed material. We call such a phenomenon the compositional instability.

Definition (Compositional Stability): In MMP, the composed material is called compositionally stable if the corresponding composition ratio function is non-decreasing and is called compositionally unstable if otherwise.

To quantify this property, we define the (2-drop) stability function as follows, with the input δ indicating the relative offset between the two droplets.

Stability Function :

$$\phi(\delta) = \min_{x\in[\delta,\ 1]} \sigma(x)\sigma'(x-\delta) - \sigma'(x)\sigma(x-\delta); \delta \in [0,1] \tag{2}$$

The value $\phi(\delta)$ is the minimum derivative of the composition ration function under a given offset δ. Therefore, to ensure the FGM with a stable gradient, we expect a non-negative value of ϕ at the given droplet offset. Otherwise, $\phi(\delta) < 0$ implies that the offset δ is unstable and leads to compositional inconsistency in FGM.

These three functions, shape function σ (describing material deposition), composition function r (describing material ratio in FGM), and stability function ϕ (determining continuous gradient or not), enable us to analyze and quantify the relationship between the droplet shape, the printing resolution, and the stability of the composed material.

2.5. Modeling of multi-drop

This subsection extends the proposed analysis framework to the more complex multi-drop setting. In this case, n droplets are printed in order with the same offset δ. So, their shape functions can be described as the set $\{\sigma(x-i\delta)\}_{i\in[n]}$, where $[n] = \{0, 1, \cdots, n-1\}$ is a finite index set. Moreover, the composition ratio linearly varies from zero to one among all droplets. This means that $r_i = \frac{i}{n-1}$ is the ratio of the second material in the ith droplet. Then, the composition ratio function for the multi-drop case is the following,

Volume Fraction of2ndMaterial :

$$r(x) = \frac{\Sigma_{i\in[n]} r_i \sigma(x-i\delta)}{\Sigma_{i\in[n]} \sigma(x-i\delta)};\ x \in [0\ , 1 + (n-1)\delta] \tag{3}$$

Then, the same definition of compositional stability applies to this multi-drop case. The corresponding multi-drop stability function can be defined as follows.

Stability Function :

$$\phi(\delta) = (n-1)^{-1} \min_{x\in[\delta,\ 1+(n-2)\delta]} \sum_{i<j\in[n]} (j-i)\widehat{\phi}(x-i\delta, (j-i)\delta) \tag{4}$$

where $\widehat{\phi}(x,\delta) = \sigma(x)\sigma'(x-\delta) - \sigma'(x)\sigma(x-\delta)$ with $\delta \in [0,1]$, $x \in [\delta, 1]$.

The intermediate function $\widehat{\phi}$ is defined only to ease the notation. It is easy to check that the 2-drop case is a special case of the above composition and stability functions for $n = 2$. Later, we will show that these functions can help to characterize the compositional gradient stability of FGM.

3. Results and discussion

3.1. Coffee-ring effect in printing

Functionally graded materials (FGMs) are important composite materials where the composition varies gradually across the volume, resulting in gradient variations in properties (e.g., thermal conductivity, strength, or magnetic permeability). As shown in Fig. 2A, the custom-built aerosol jet printer fabricates FGMs by continuously varying the deposition of two inks through controlled atomization and gas flow. The sheath flow focuses on the aerosol stream, ensuring high-resolution deposition. Monotonic variation in material composition (i.e., changing material composition from one to another monotonically, if not linearly) is achieved by adjusting the ink ratio during printing, creating smooth transitions between materials. In ink-based printing of FGMs, understanding material gradient effects (e.g., stability) is essential for optimizing ink deposition and drying processes. Uneven drying of the inks causes a flow that carries dispersed nanomaterials toward the edges, often leaving the center with minimal material.

To quantify the drying effect on printing FGM, we first prepare inks of different materials, including metals (Ag), semiconductors (Bi_2Te_3), and ceramics (halloysite and kaolinite). Fig. 2B shows examples of coffee-ring effects from drop-casted ink, demonstrating a wide variety of shapes of ink droplets after drying, highlighting the complexity and diversity of ink drying process. This complexity is due to the fact that solvent, deposition temperature [20], particle surface charge (zeta potential) [21,22], particle size [23], concentration [24], etc. can affect the drying kinetics and lead to different shape functions. While the printhead travels through the substrate line by line, a "two-peak" shape from the coffee-ring effect is shown in Fig. 2C. In both cases, the deposition leaves the center with fewer materials, which becomes worse when

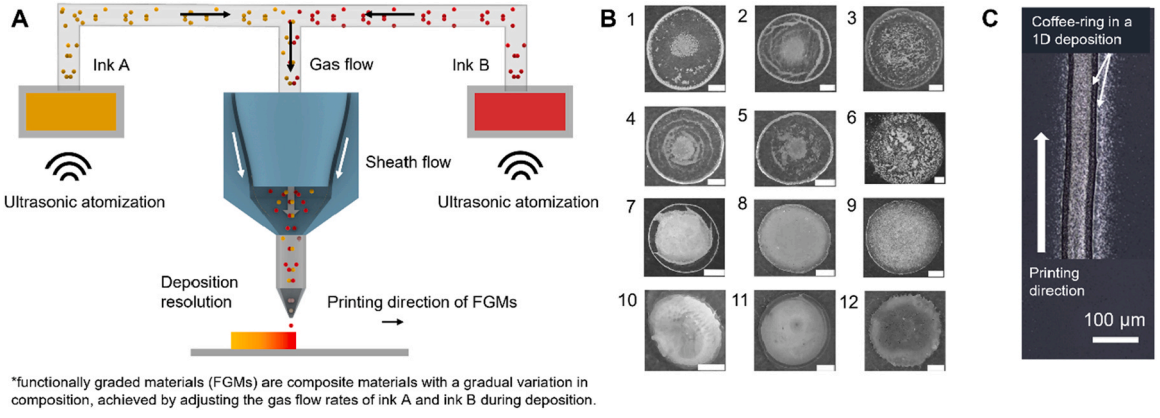

Fig. 2. Multi-material printing and coffee-ring effect. A) Schematics showing the multi-material aerosol-jet printing of functionally graded materials, requiring a monotonic shift in material composition. B) Examples of the coffee-ring effect observed with various drop-casted ink formulations, illustrating the common occurrence of unwanted drying phenomena. Coffee-ring effect on different suspensions. (**1–3**) 1 wt% halloysite nanoclay with 5 wt% EG, 15 wt% EG aqueous solution, and pure acetone, respectively; (**4–6**) 1 wt% kaolinite with 5 wt% EG, 15 wt% EG aqueous solution, and pure acetone, respectively; (**7–9**) 1 wt% Bi_2Te_3 with 5 wt% EG, 15 wt% EG aqueous solution, and pure acetone, respectively; (**10–12**) 1 wt% Ag nanoink with 5 wt% EG, 15 wt% EG aqueous solution, and pure acetone, respectively. Scales are 1 mm. C) Optical microscopic image of the AJP-printed single line (1D deposition) showing coffee-ring effect. Gradient thin films consist of multiple lines with gradual changes in material composition.

varying deposition composition during the printing of FGM. To understand and possibly address this unwanted and common challenge in ink printing, we propose a mathematical model to quantify how this drying-oriented deposition variation affects the composition gradients in printed FGM.

3.2. Shape effect on 2-drop

In our mathematical model, we consider the printing of FGM from two different inks (i.e., ink A and ink B), where the model will predict whether a monotonic variation in FGM is achieved (monotonic change in volume fraction of B) with a given shape function of the dried droplet. Fig. 3 illustrates three different types of shape functions. The first two are functions fitted from the experiment data using spline regression [40–42], both of which exhibit different types of coffee-ring effects, while the last one is a computer-generated symmetric and concave-shaped function (i.e., no coffee-ring effect) for comparison. The bottom figures are the composition ratio functions $r(\cdot)$ (which is correspond to the experimentally measured volume fraction of secondary materials in FGM) associated with each shape function under the same offset $\delta = 0.3$. Each droplet offset δ induces a distinct composition ratio function. The stability function then computes the minimum first-order derivative of this composition ratio function for the given δ. A non-negative output indicates that the composition function is stable (non-decreasing), while a negative value suggests decreasing regions, which could lead to printing instability. Therefore, this stability function helps identify printing resolutions that are stable.

When there is no coffee-ring effect for drops (Fig. 3C), an increasing $r(\cdot)$ (Fig. 3F) indicates a smooth transition in material composition and thus is called compositionally stable. In contrast, the coffee-ring effects exhibited in Fig. 3A and B caused the oscillating behaviors of the corresponding ratio functions for the specific offset $\delta = 0.3$ (the defined deposition resolution between each print pass). Moreover, compared to Fig. 3A, the drastic coffee-ring effect illustrated in Fig. 3B also led to a more pronounced instability shown in Fig. 3E.

Therefore, searching for the theoretical optimal printing resolution (smallest offset δ) under compositional gradient stability becomes critical for ink-based MMP tasks. The following conclusions provide convenient tools for such purposes. The corresponding technical derivations and proofs can be found in the Supplementary Information.

Main Results for 2-Drop: For a given droplet shape function σ, let ϕ be the corresponding stability function, we have the following results.

1. The composed material with an offset distance δ is compositionally stable if and only if $\phi(\delta) \geq 0$.
2. The gradient of composed material is compositionally stable regardless of the offset if the shape function satisfies $(\sigma'(x))^2 \geq \sigma''(x)\sigma(x)$ for all $x \in [0,1]$. In particular, concave-shaped droplets are always stable.
3. For symmetric droplets with two peaks, the minimum offset to ensure compositional gradient stability is $\delta = 1 - 2p$, where p is the location of the first peak in the shape function.

The first result implies that the stability function ϕ can be used to optimize the MMP resolution. The second result confirms the observations in experiments that concave-shaped droplets always have good stability properties (as seen in Fig. 3F), even under a high resolution. The last result provides a convenient tool to quickly determine a stable resolution if the droplets have a symmetric shape with two peaks. Intuitively speaking, the stable resolution is quite low if the two peaks are widely separated and becomes high when the two peaks are close to each other.

Fig. 4A–C illustrate the stability functions associated with the three shapes presented in Fig. 3. The two axes represent the input offset δ and the output value $\phi(\delta)$, respectively. The red dotted lines represent the constant function of zero. According to the main results, compositional gradient stability is guaranteed if and only if $\phi(\delta) \geq 0$. Thus, the minimum δ with a nonnegative output $\phi(\delta)$ is the smallest offset that ensures stability. The split point of the first shape is around 0.53: any smaller offset is unstable, while larger ones are stable. The situation becomes more complicated for the second shape. In Fig. 4B, a stable offset can be first found around 0.51, but this point is very sensitive to small

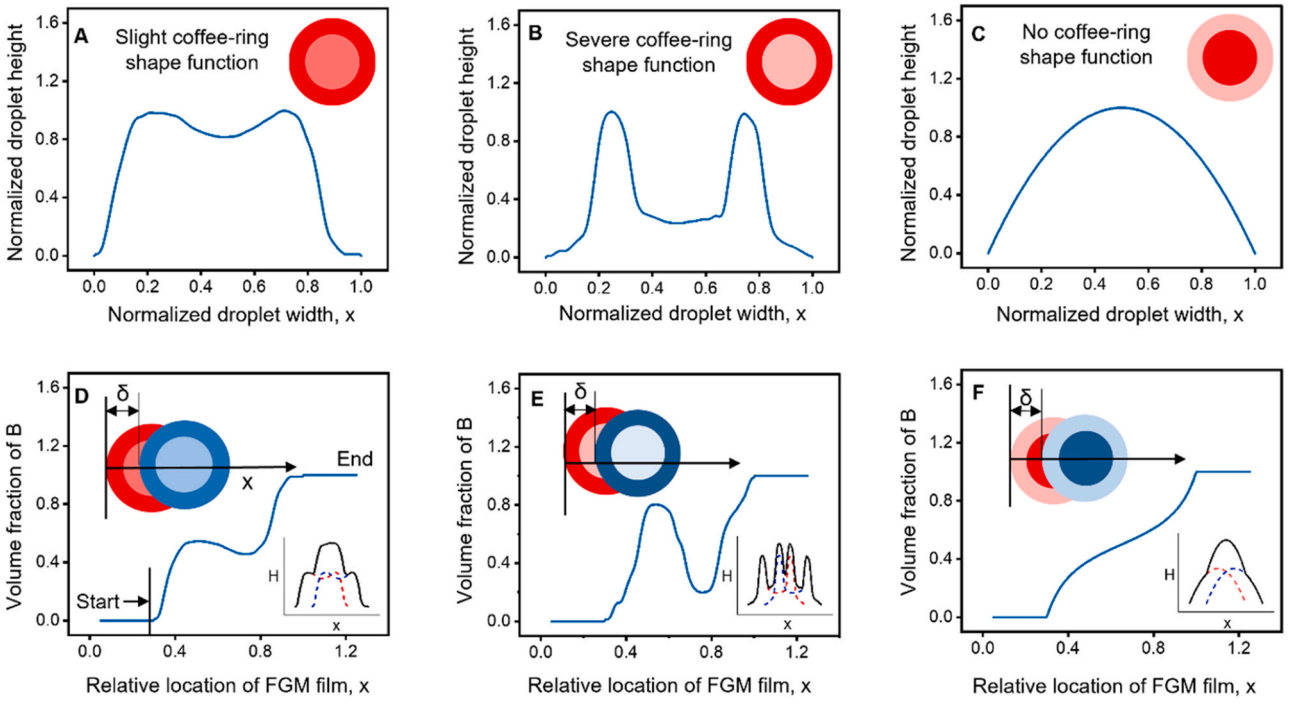

Fig. 3. Shape functions of coffee-ring effect and their impact on compositional monotonicity of gradient materials. (A–C) Shape functions of deformed (slight coffee-ring) (A), spread (severe coffee-ring) (B), and ideal cases (no coffee-ring) (C) and their composition ratio functions (bottom three D–F) with a deposition interval (offset) of 0.3. In inset, H is the height of combined droplet.

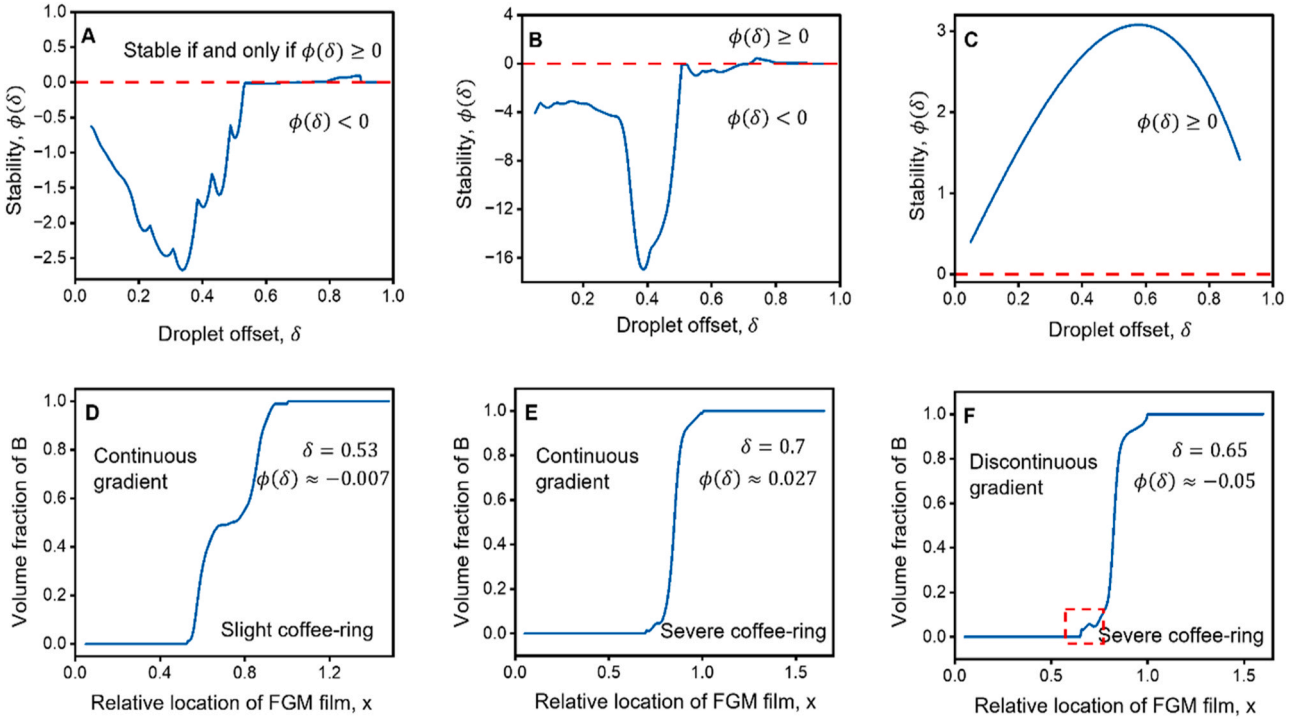

Fig. 4. Top three (A–C): stability functions of the three shapes (slight coffee-ring, severe coffee-ring and no coffee-ring). Bottom three (D–F), the composition ratio functions where D corresponds to the slight coffee-ring shape with an offset $\delta = 0.53$, E and F correspond to the severe coffee-ring shape with offsets $\delta = 0.7$ and 0.65, respectively. Note that both D and E are increasing functions, while F has a decreasing trend around 0.75.

perturbations as it barely touches the zero line. A more robust choice could be at any point after 0.7. In contrast, the entire stability function $\phi(\cdot)$ is above the zero line for the third concave-shaped droplet, implying that the printing resolution would not affect the material compositional gradient stability in this case.

These observations are consistent with Fig. 3D-F where the offset is fixed at the value of 0.3: since the value $\phi(0.3)$ is below zero in both Fig. 4A and B, Fig. 3D and E indicate that the composed material is unstable; the value $\phi(0.3)$ is positive in Fig. 4C; hence the composition function in Fig. 3F is strictly increasing, confirming a compositionally stable printing process. On the other hand, when taking the offset $\delta = 0.53$ and 0.7 for the first two shapes, the corresponding composition functions are both increasing as shown in Fig. 4D and E, which are consistent with the positive values of $\phi(\delta)$ in the stability functions shown in Fig. 4A and B. However, when setting $\delta = 0.65$ for the second shape, we have $\phi(\delta) < 0$ in Fig. 4B, thus the associated composition function in Fig. 4F has a decreasing segment around the point 0.75.

Another interesting observation demonstrated in Fig. 4 is the usefulness of the third main result. The first peak in Fig. 3A is approximately located at $p = 0.21$. By the third result, the minimum offset is obtained at $\delta = 1 - 2p = 0.58$. Similarly, the first peak in Fig. 3B is around $p = 0.22$, which gives a stable point δ at 0.56. Both are close approximations of the results observed in Fig. 4.

3.3. Shape effect on multi-drop

In this case, multiple droplets with the same cross-section shape function are printed subsequently. That is, to print n droplets, the shape function of the ith drop is described by $\sigma(x - i\delta)$ for each $i \in [n]$. Moreover, each droplet is composed of two materials with the ratio of the second material as $r_i = \frac{i}{n-1}$. Then, we have the following main results for this multi-drop setting.

Main Results for Multi-Drop: For a given droplet shape function σ, let ϕ be the corresponding (multi-drop) stability function, we have the following results.

1. The gradient composite material with an offset distance δ is compositionally stable (i.e., a continuous gradient will form) if and only if $\phi(\delta) \geq 0$.
2. The gradient composite material is compositionally stable regardless of the offset if the shape function satisfies $(\sigma'(x))^2 \geq \sigma''(x)\sigma(x)$ for all $x \in [0, 1]$. In particular, concave-shaped droplets are always stable (i.e., a continuous gradient will always form if the droplet shape function is concave).

Again, the first result states that the multi-drop stability function $\phi(\delta)$ exactly characterizes the compositional stability for all $\delta \in [0, 1]$, and the second result confirms that the concave-shaped droplet is still stable for arbitrary resolution even in this multi-drop setting. Similar as in the 2-drop case, this multi-drop version of stability function computes the minimum first-order derivative of the composition function for every given δ. Then, non-negative or negative outputs indicate the stability of the associated composition function. Hence, it helps identify stable printing resolutions in this multi-drop case.

Fig. 5 illustrates the multi-drop stability functions for the three shapes in Fig. 3A–C. Compared to their 2-drop counterparts shown in Fig. 4A–C, the multi-drop stability functions in Fig. 5 demonstrate more complex patterns. We clearly have many more peaks and valleys in all three functions. Moreover, in Fig. 5A, it is surprising to observe some positive points before $\delta = 0.17$, which were all negative in Fig. 4A. This indicates that for certain shapes, a sufficiently small offset (sufficiently large resolution) may overcome the compositional instability caused by the coffee-ring effects. However, this phenomenon is not displayed in Fig. 5B for the second shape, where the stable offsets are similar to its 2-drop counterpart shown in Fig. 4B. For the last concave-shaped droplet, though its stability function in Fig. 5C is more complex than its 2-drop counterpart in Fig. 4C, all the points are still above the zero line, which confirms the second main result for the multi-drop case.

Fig. 6 illustrates the multi-drop composition functions for the first two shapes in Fig. 3. The top three (Fig. 6A–C) correspond to the first shape with offsets $\delta = 0.15, 0.4, 0.7$, while the bottom three (Fig. 6D–F)

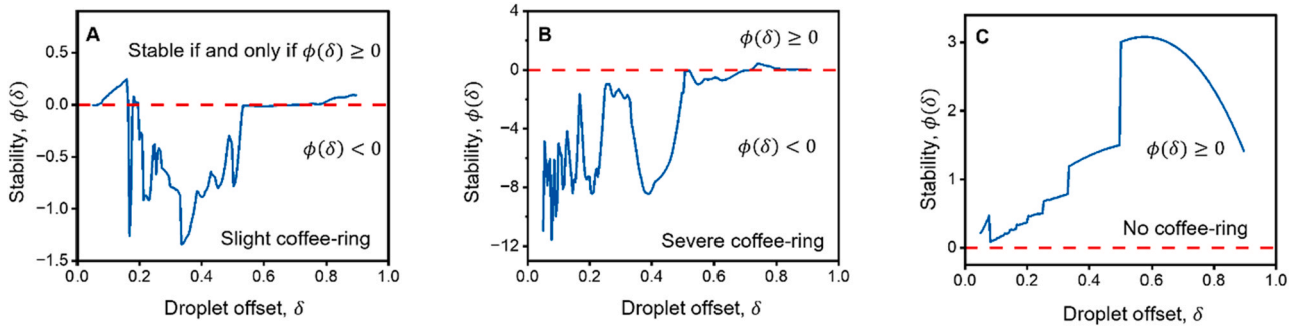

Fig. 5. Multi-drop stability functions for the three shapes in Fig. 3**A–3 C.** (A) Slight coffee-ring, (B) severe coffee-ring and (C) no coffee-ring effect. The compositional gradient stability is guaranteed if and only if $\phi(\delta) \geq 0$, otherwise unstable.

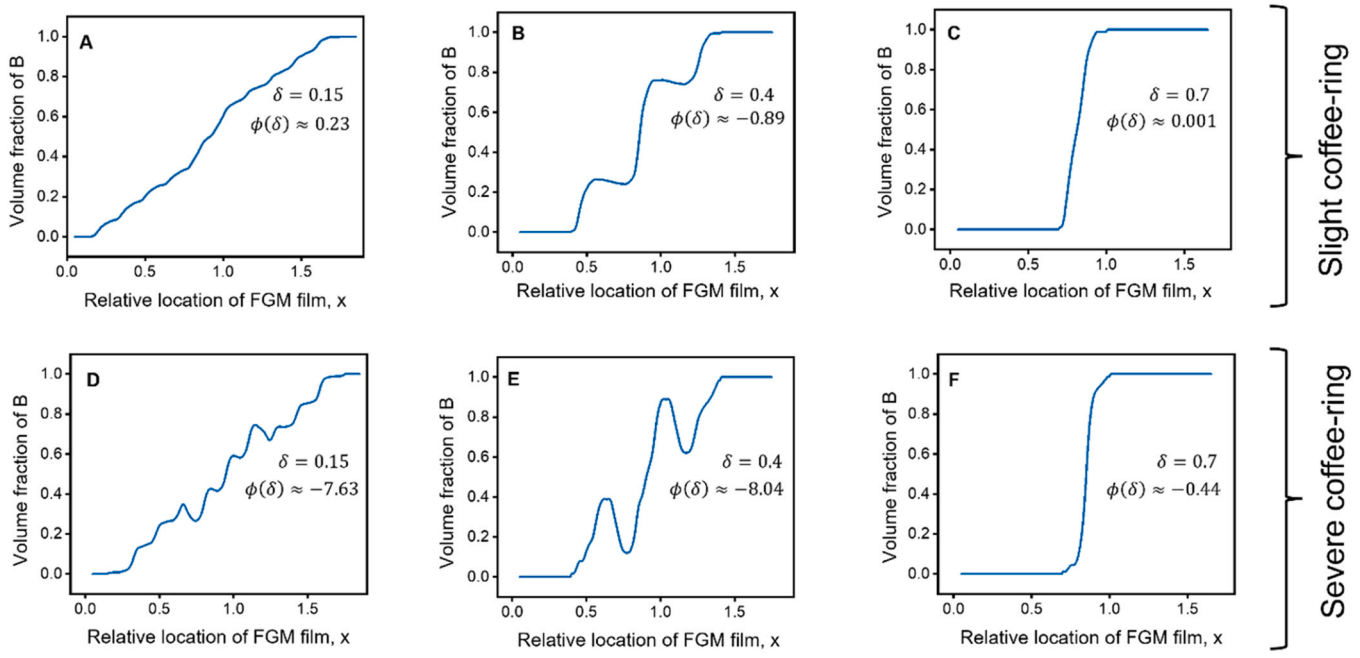

Fig. 6. Multi-drop composition functions. The top row for the slight coffee-ring effect with (A) offset, $\delta = 0.15$; (B) offset, $\delta = 0.4$, (C) offset, $\delta = 0.7$, respectively. The bottom row for the severe coffee-ring with (D) offset, $\delta = 0.15$; (E) offset, $\delta = 0.4$, (F) offset, $\delta = 0.7$, respectively.

are for the second shape with the same set of offsets. For $\delta = 0.15$, the composition function for shape one is strictly increasing, implying a stable MMP process; in contrast, the composition function for shape two has multiple decreasing sections, which renders an unstable process. For $\delta = 0.4$, both curves have clear decreasing segments, though the second shape demonstrates significant variations due to its severe coffee-ring effect. For $\delta = 0.7$, both curves are strictly increasing, showing a relatively smooth transition in their composition (i.e., a continuous gradient). All these results are consistent with the polarity (positivity or negativity) presented in Fig. 5A and B.

The coffee-ring effect can be influenced by various factors such as temperature, drying time, ink properties etc., leading to a more complex shape upon drying. To clarify our model, we also present an example of detailed workflow, as shown in Fig. 7. The model begins by identifying the shape function derived from the dried droplet profile, followed by predicting an offset that enables a stable, continuous increase in the concentration of the secondary hypothetical material B. Based on the stability function, our predictions indicate that an offset of 0.4 results in an unstable composition of material B, while an offset of 0.75 yields a stable composition. We subsequently validate these offset predictions, where the difference in printing offset (0.4 vs 0.75) indeed significantly affects the FGM material composition.

To demonstrate the robustness of our model, we evaluate two additional examples of complex shape functions as shown in Fig. 8**.** From the stability functions associated with the first complex shape, we observe positive points around offset, $\delta = 0.9$, means for this shape a large offset value may overcome the compositional instability **(**Fig. 8A-B). As shown in Fig. 8C and D, the material transition is smoother at $\delta = 0.9$ than $\delta = 0.8$. In Fig. 8E–H, we have provided another example of a complex shape function, where at small offsets, $\delta = 0.3$ and $\delta = 0.4$ both showed an almost monotonic increase in the composition as predicted by stability functions. Thus, rather than using large offsets, the model can optimize the printing resolution for the second shape at high resolution (e.g., low offset value).

3.4. Experimental verification

To evaluate our approach during multi-material printing, we used bismuth telluride (Bi_2Te_3) nanoink as a model example where the composition of printed FGM samples can be controlled by gradually increasing the Ag ink amount (formation of Bi_2Te_3-Ag gradient composite). We first measured the shape function of nanoparticle inks. As shown in Fig. 9, a typical ink formulation shows the coffee-ring effect of the drying process. We also systematically investigate the processing

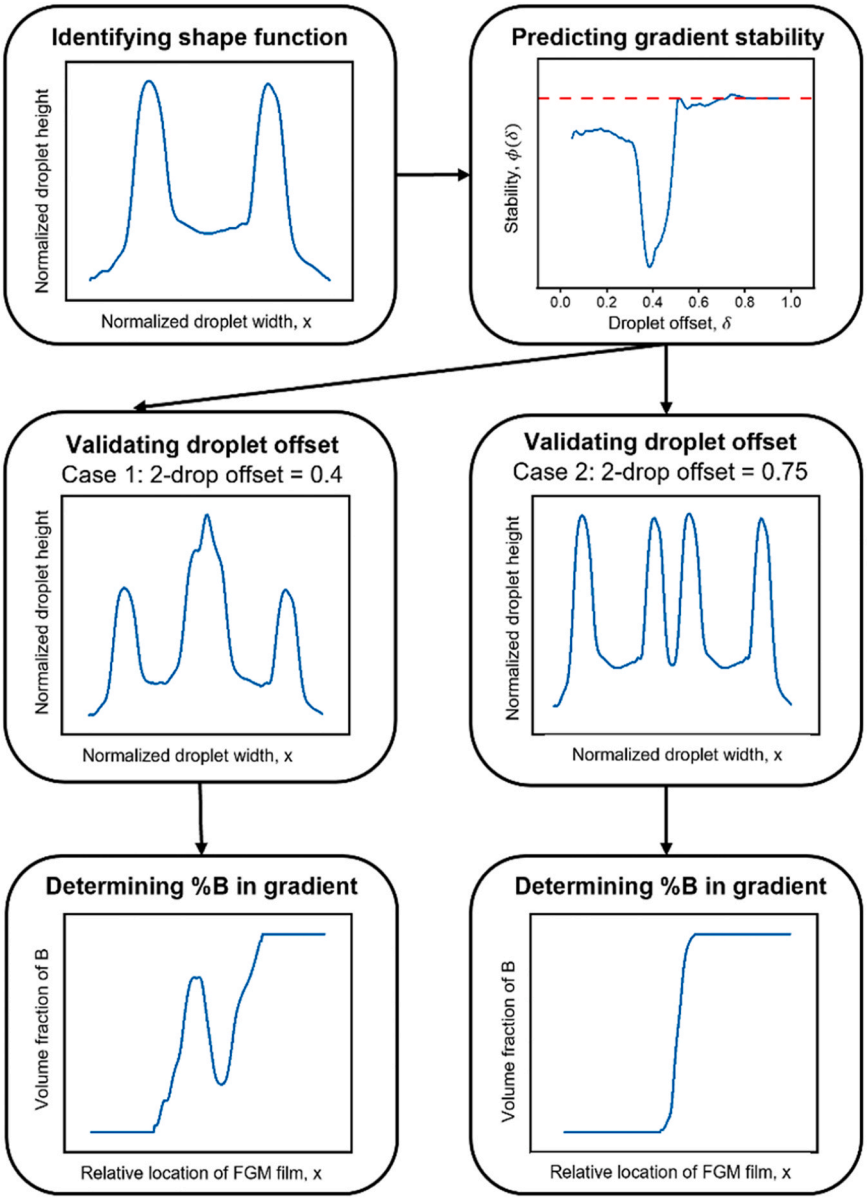

Fig. 7. Example workflow of the drying-oriented resolution optimization (DORO) model for dried droplets.

variables (ink composition and sheath flow) on the printed samples. As shown in Fig. 9, the comparison of the coffee-ring effect is presented through thickness mapping of printed lines from two Bi_2Te_3 ink formulations: one without ethylene glycol (EG) (Fig. 9A) and with EG (Fig. 9B). The inclusion of EG notably minimizes the spreading of printed droplets due to Marangoni flow effect, leading to more uniform material deposition with less severe coffee-ring effect (Fig. 9C). Additionally, the influence of sheath flow rate on the dispersion of printed water-based inks is examined (Fig. 9D), highlighting how aerodynamics can lead to a narrowing of the droplet during the printing process and consequently a less spreading in shape functions.

As the EG can help mitigate the overspreading of the ink, we prepared EG-based inks (Bi_2Te_3 and Ag) to showcase the effect of printing step width on the stability of the compositional gradient, where the Ag was gradually added into Bi_2Te_3 materials during the multi-material printing process. The use of heavy-atom Bi_2Te_3 and Ag is to reduce the measurement uncertainty during the elemental analysis using energy-dispersive X-ray spectroscopy (EDX). To accurately measure the composition of gradient film using EDX, many studies have suggested that heavy atoms (e.g., Bi, Te, Ag) can significantly reduce the measurement uncertainty in comparison with other light elements (such as C, N, O, Si) [43]. With EG-based ink, we tested two cases where the offset of each deposition path (also referred to as printing step width or printing resolution for other additive manufacturing processes) was set to 10 μm and 25 μm. As shown in Fig. 10A-B, the elemental analysis using EDX revealed that a small printing step leads to an unstable material gradient, while a relatively large printing step showed a more consistent composition gradient (i.e., monotonic increasing or decreasing trend). Such experimental observation is aligned with our calculation prediction over the shape function of printed nanoinks, where a higher offset value (δ) will favor the gradient compositional monotonicity/stability (though not 100 % matching numerically due to the potential difference between experimental deposition and droplet modeling). In a more complex experimental case, we use an optical profilometer to quantify the shape function of a typical printed line (Fig. 10C); upon increasing the deposition offset, the compositional gradient stability slowly increases from very unstable (Fig. 10D-E) to more stable trend (Fig. 10F), where the increasing trend of volume fraction (additive phase) gradually stabilize.

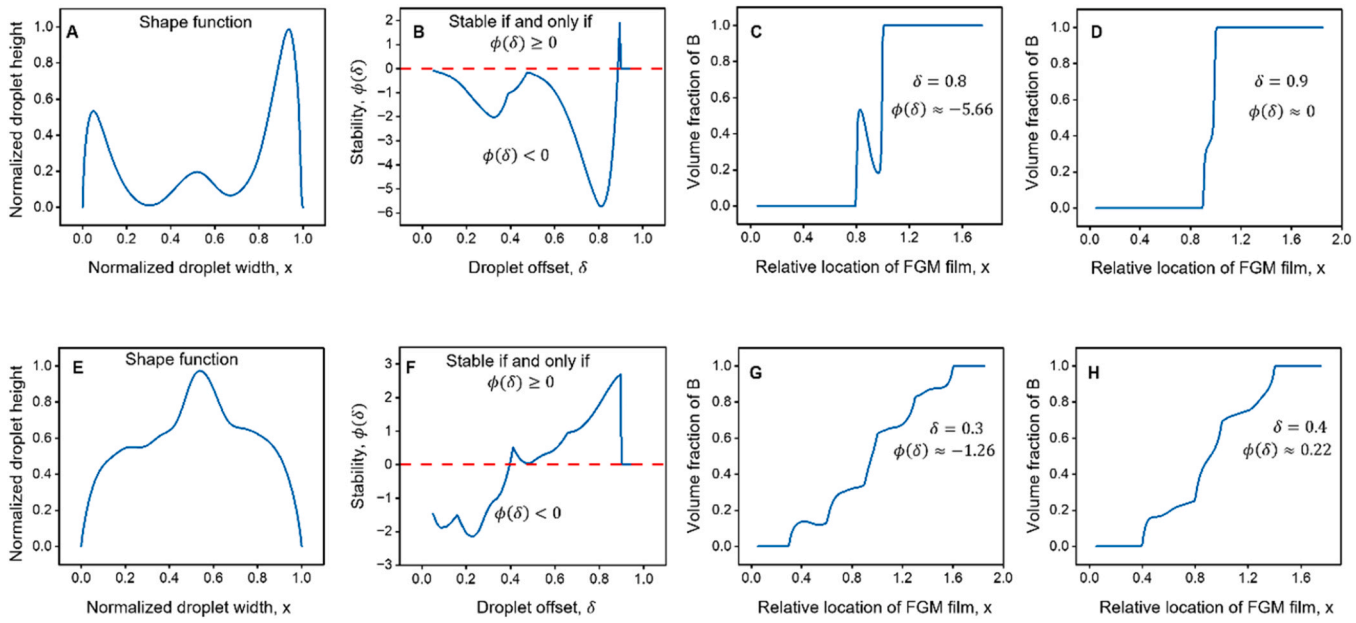

Fig. 8. Examples of complex shape functions from drying. (A) Shape function for multi-peak shape, (B) stability function corresponds to the shape, (C) composition function with unstable offset $\delta = 0.8$ and (D) composition function with stable offset $\delta = 0.9$ found from the stability function for that shape; (E) Shape function for asymmetric shape from drying, (F) stability function corresponds to the shape, (G) composition function with unstable offset $\delta = 0.3$ and (H) composition function with stable offset $\delta = 0.4$ found from the stability function for that shape respectively.

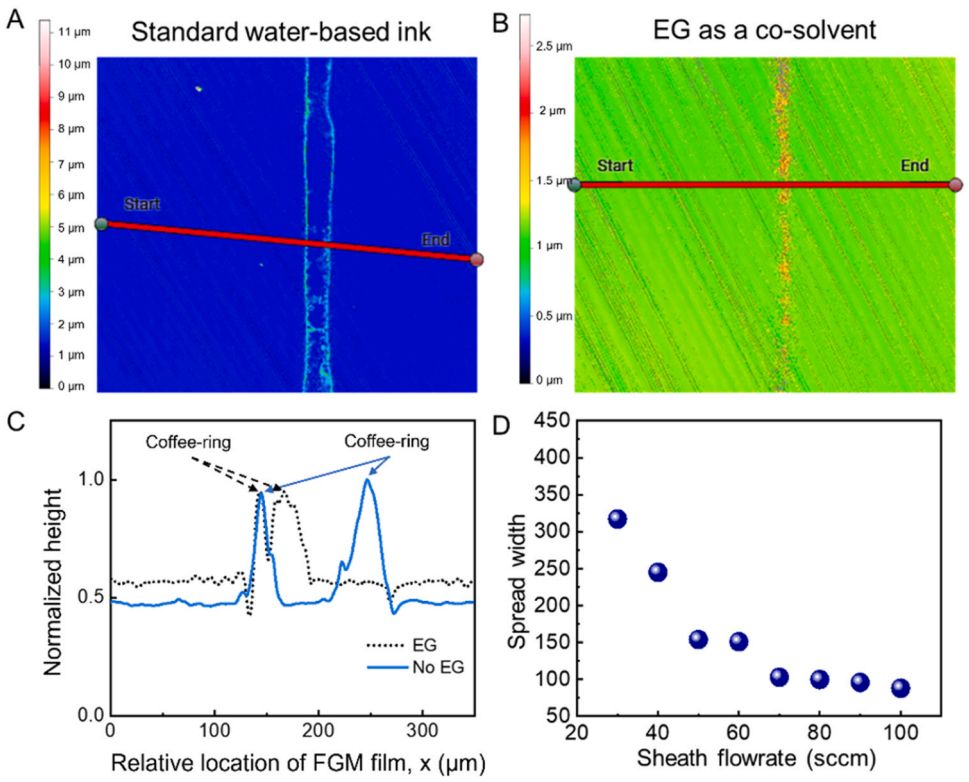

Fig. 9. Rich physics in drying shapes and shape functions controlled by various processing variables (ink composition and sheath flow). (A-B) The thickness mapping of the printed line with a single pass without (A) and with EG (B) in inks. (C). The profile of the coffee-ring effect where EG can significantly reduce the spread of printed droplets. (D) The effect of sheath flowrate on the spread of printed water-based inks (spread width in μm), revealing the aerodynamic narrowing of droplets during printing.

4. Conclusion

In summary, we propose a model to describe the role of the drying effect on materials composition uncertainty and suggest the DORO framework for gradient composition optimization (i.e., estimating the optimal printing resolution related to shape function of ink droplets). Various parameters, including concavity and shape features, have been considered and compared for optimized compositional gradient

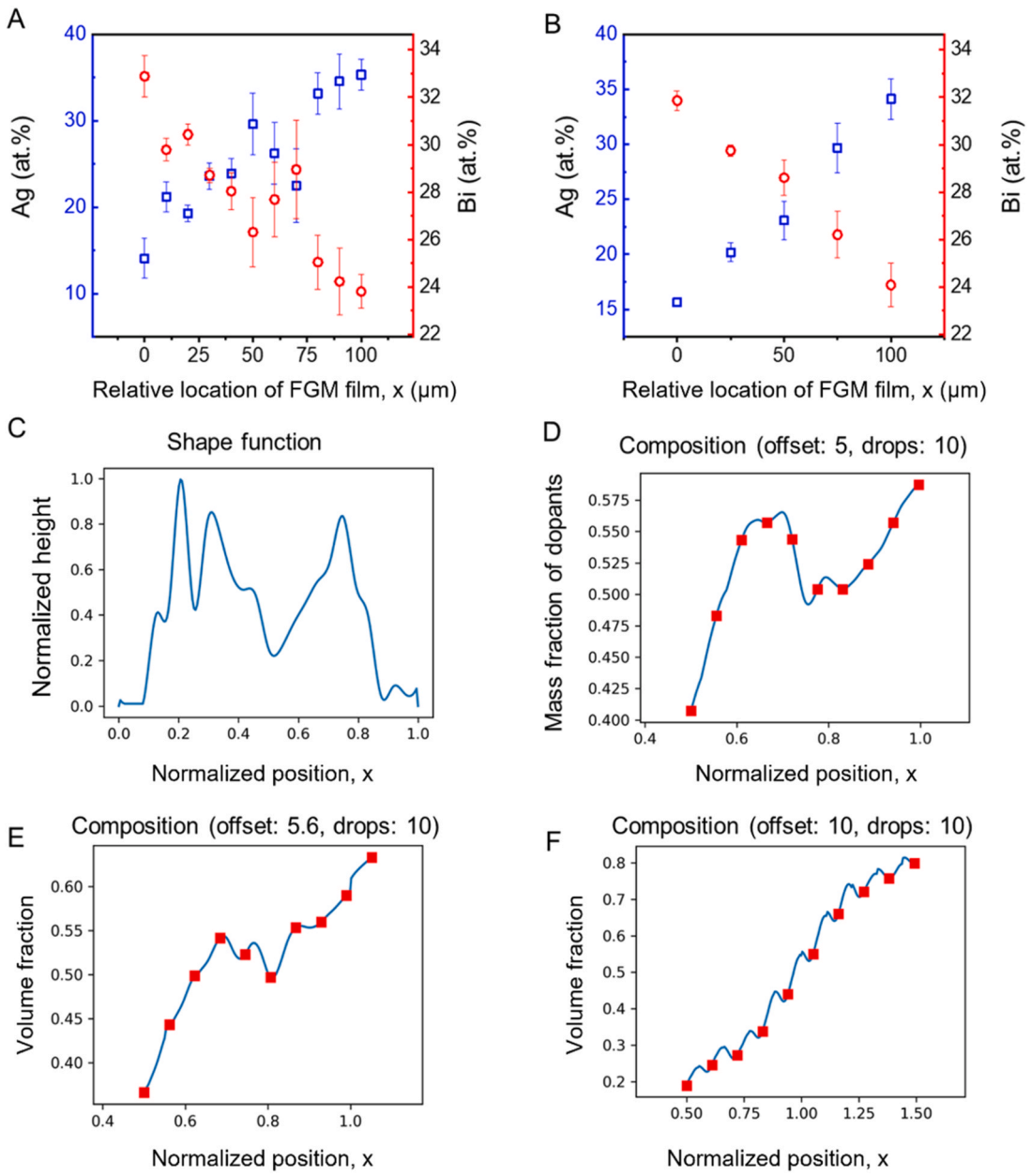

Fig. 10. Experimental observation and model comparison of printed gradient materials. (A-B) Elemental analysis using EDX shows gradient uncertainty at different printing line gaps (10 μm and 25 μm, leads to different offset value), indicating larger line gaps are preferred for monotonic deposition. Error bars represent the standard deviation of atomic concentration. (C) Optical profilometer measurement of the shape function for a printed line. (D-F) Validation of gradient uncertainty under different drop-to-drop resolutions (i.e., offset), suggesting an increase in monotonicity with higher offset values. The units of offsets in D-F are in μm.

stability. Compared with ideal depositions with no undesired drying, it was found that the coffee-ring pattern is able to impose a non-negligible uncertainty over the material composition of FGM systems, while such effects on the edge are particularly profound for multi-material deposition from our two-drop model. This coffee-ring-induced composition variability is further exaggerated with higher valley curvature. In addition, such findings can be extended to estimate the optimal printing offset for printing compositionally graded materials for minimal instability in composition gradient. As we assume that the printing process is ideal with each step taking the same offset, future research is needed for considering the variability factors such as changing offset and deposition error. By considering those factors, it is expected that this model will help optimize printing parameters such as printing offset in additive manufacturing of FGM in terms of material stability [44–47].

CRediT authorship contribution statement

Yanliang Zhang: Writing – review & editing, Validation. **Minxiang Zeng:** Writing – review & editing, Supervision, Conceptualization. **Ningji Wei:** Methodology, Data curation, Conceptualization. **Hur-E-Jannat Moni:** Writing – original draft, Investigation, Formal analysis, Data curation. **Qiang Jiang:** Investigation, Data curation.

Declaration of Competing Interest

The authors declare that they have no known competing financial interests or personal relationships that could have appeared to influence the work reported in this paper.

Acknowledgements

N.W. and M.Z. thank the support of Texas Tech Startup Funds. M. Z. also acknowledges the support from the NSF (Grant No. DMR-2418915).

Appendix A. Supporting information

Supplementary data associated with this article can be found in the online version at doi:10.1016/j.addma.2024.104609.

Data availability

Data will be made available on request.

References

[1] D.A. Rau, C.B. Williams, M.J. Bortner, Rheology and printability: A survey of critical relationships for direct ink write materials design, Prog. Mater. Sci. 140 (2023) 101188, https://doi.org/10.1016/j.pmatsci.2023.101188.
[2] M. Zeng, Y. Zhang, Colloidal nanoparticle inks for printing functional devices: emerging trends and future prospects, 10.1039/C9TA07552F, J. Mater. Chem. A 7 (41) (2019) 23301–23336, https://doi.org/10.1039/c9ta07552f.
[3] M. Zeng, D. Zavanelli, J. Chen, M. Saeidi-Javash, Y. Du, S. LeBlanc, G.J. Snyder, Y. Zhang, Printing thermoelectric inks toward next-generation energy and thermal devices, 10.1039/D1CS00490E, Chem. Soc. Rev. 51 (2) (2022) 485–512, https://doi.org/10.1039/D1CS00490E.
[4] M.A. Skylar-Scott, J. Mueller, C.W. Visser, J.A. Lewis, Voxelated soft matter via multimaterial multinozzle 3D printing, Nature 575 (7782) (2019) 330–335, https://doi.org/10.1038/s41586-019-1736-8.
[5] R. Wick-Joliat, M. Schroffenegger, D. Penner, Multi-material ceramic material extrusion 3D printing with granulated injection molding feedstocks, Ceram. Int. 49 (4) (2023) 6361–6367, https://doi.org/10.1016/j.ceramint.2022.10.170.
[6] Y. Zhai, Z. Wang, K.S. Kwon, S. Cai, D.J. Lipomi, T.N. Ng, Printing multi-material organic haptic actuators, Adv. Mater. 33 (19) (2021) 2002541.
[7] M.Y. Teo, S. Kee, L. Stuart, J. Stringer, K.C. Aw, Printing of covalent organic frameworks using multi-material in-air coalescence inkjet printing technique, J. Mater. Chem. C. 9 (36) (2021) 12051–12056.
[8] J. Chen, M. Saeidi-Javash, M. Palei, M. Zeng, Y. Du, K. Mondal, M.D. McMurtrey, A.J. Hoffman, Y. Zhang, Printing noble metal alloy films with compositional gradient, Appl. Mater. Today 27 (2022) 101405.
[9] Y. Du, R. Wang, M. Zeng, S. Xu, M. Saeidi-Javash, W. Wu, Y. Zhang, Hybrid printing of wearable piezoelectric sensors, Nano Energy 90 (2021) 106522, https://doi.org/10.1016/j.nanoen.2021.106522.
[10] M. Zeng, W. Kuang, I. Khan, D. Huang, Y. Du, M. Saeidi-Javash, L. Zhang, Z. Cheng, A.J. Hoffman, Y. Zhang, Colloidal nanosurfactants for 3D conformal printing of 2D van der Waals materials, Adv. Mater. 32 (39) (2020) 2003081.
[11] M. Saeidi-Javash, Y. Du, M. Zeng, B.C. Wyatt, B. Zhang, N. Kempf, B. Anasori, Y. Zhang, All-printed MXene–graphene nanosheet-based bimodal sensors for simultaneous strain and temperature sensing, ACS Appl. Electron. Mater. 3 (5) (2021) 2341–2348.
[12] M. Zeng, Y. Du, Q. Jiang, N. Kempf, C. Wei, M.V. Bimrose, A. Tanvir, H. Xu, J. Chen, D.J. Kirsch, High-throughput printing of combinatorial materials from aerosols, Nature 617 (7960) (2023) 292–298.
[13] M. Teacher, R. Velu, Additive manufacturing of functionally graded materials: A comprehensive review, Int. J. Precis. Eng. Manuf. 25 (1) (2024) 165–197.
[14] C. Zhang, F. Chen, Z. Huang, M. Jia, G. Chen, Y. Ye, Y. Lin, W. Liu, B. Chen, Q. Shen, et al., Additive manufacturing of functionally graded materials: A review, Mater. Sci. Eng.: A 764 (2019) 138209, https://doi.org/10.1016/j.msea.2019.138209.
[15] R. Ghanavati, H. Naffakh-Moosavy, Additive manufacturing of functionally graded metallic materials: A review of experimental and numerical studies, J. Mater. Res. Technol. 13 (2021) 1628–1664, https://doi.org/10.1016/j.jmrt.2021.05.022.
[16] E.B. Secor, Principles of aerosol jet printing, Flex. Print. Electron. 3 (3) (2018) 035002, https://doi.org/10.1088/2058-8585/aace28.
[17] Goh, G.L.; Agarwala, S.; Yeong, W.Y. High resolution aerosol jet printing of conductive ink for stretchable electronics. 2018.
[18] N. Wilkinson, M. Smith, R. Kay, R. Harris, A review of aerosol jet printing—a non-traditional hybrid process for micro-manufacturing. Int. J. Adv. Manuf. Technol. 105 (2019) 4599–4619.
[19] N.J. Wilkinson, M.A.A. Smith, R.W. Kay, R.A. Harris, A review of aerosol jet printing—a non-traditional hybrid process for micro-manufacturing, Int. J. Adv. Manuf. Technol. 105 (11) (2019) 4599–4619, https://doi.org/10.1007/s00170-019-03438-2.
[20] K. Sefiane, Patterns from drying drops, Adv. Colloid Interface Sci. 206 (2014) 372–381.
[21] K.N. Al-Milaji, H. Zhao, New Perspective of mitigating the coffee-ring effect: Interfacial assembly, J. Phys. Chem. C. 123 (19) (2019) 12029–12041.
[22] M. Anyfantakis, Z. Geng, M. Morel, S. Rudiuk, D. Baigl, Modulation of the coffee-ring effect in particle/surfactant mixtures: the importance of particle–interface interactions, Langmuir 31 (14) (2015) 4113–4120.
[23] L. Bansal, P. Seth, B. Murugappan, S. Basu, Suppression of coffee ring:(Particle) size matters, Appl. Phys. Lett. 112 (21) (2018).
[24] D. Lohani, M.G. Basavaraj, D.K. Satapathy, S. Sarkar, Coupled effect of concentration, particle size and substrate morphology on the formation of coffee rings, Colloids Surf. A: Physicochem. Eng. Asp. 589 (2020) 124387.
[25] B. Ji, L. Zhang, M. Li, S. Wang, M.-K. Law, Y. Huang, W. Wen, B. Zhou, Suppression of coffee-ring effect via periodic oscillation of substrate for ultra-sensitive enrichment towards surface-enhanced Raman scattering, Nanoscale 11 (43) (2019) 20534–20545.
[26] S.K. Saroj, P.K. Panigrahi, Magnetic suppression of the coffee ring effect, J. Magn. Magn. Mater. 513 (2020) 167199.
[27] B. Fan, J. Xiong, Y. Zhang, C. Gong, F. Li, X. Meng, X. Hu, Z. Yuan, F. Wang, Y. Chen, A bionic interface to suppress the coffee-ring effect for reliable and flexible perovskite modules with a near-90% yield rate, Adv. Mater. 34 (29) (2022) 2201840.
[28] G.K. Raghuram, L. Bansal, S. Basu, A. Kumar, Suppression of coffee ring effect in high molecular weight polyacrylamide droplets evaporating on hydrophobic surfaces, Colloids Surf. A Physicochem. Eng. Asp. 612 (2021) 126002.
[29] S. Shahruddin, N. Ideris, N.A. Bakar, A. Ahmad, N. Lah, Influence of membrane character on suppression of coffee-ring effect, Mater. Today.: Proc. 46 (2021) 1870–1874.
[30] Z. Du, H. Zhou, X. Yu, Y. Han, Controlling the polarity and viscosity of small molecule ink to suppress the contact line receding and coffee ring effect during inkjet printing, Colloids Surf. A Physicochem. Eng. Asp. 602 (2020) 125111.
[31] D.A. Chalkias, A. Mourtzikou, G. Katsagounos, A. Karavioti, A.N. Kalarakis, E. Stathatos, Suppression of Coffee-Ring Effect in Air-Processed Inkjet-Printed Perovskite Layer toward the Fabrication of Efficient Large-Sized All-Printed Photovoltaics: A Perovskite Precursor Ink Concentration Regulation Strategy, Sol. RRL 6 (8) (2022) 2200196.
[32] J. Hu, Z. Xu, K. Yuan, C. Shen, K. Xie, B. Wei, Understanding the coffee ring effect on self-discharge behavior of printed micro-supercapacitors. Energy Environ. Mater. 5 (1) (2022) 321–326.
[33] D. Soltman, V. Subramanian, Inkjet-printed line morphologies and temperature control of the coffee ring effect, Langmuir 24 (5) (2008) 2224–2231, https://doi.org/10.1021/la7026847.
[34] J. Niu, L. Qi, H. Lian, J. Luo, R. Zhang, X. Chao, Revisiting the inhomogeneity in drop-on-demand printing of graphene: An effective route for overcoming the coffee-ring effect, Surf. Interfaces 46 (2024) 104036, https://doi.org/10.1016/j.surfin.2024.104036.
[35] S. Lu, J. Zheng, J.A. Cardenas, N.X. Williams, Y.-C. Lin, A.D. Franklin, Uniform and Stable Aerosol Jet Printing of Carbon Nanotube Thin-Film Transistors by Ink Temperature Control, ACS Appl. Mater. Interfaces 12 (38) (2020) 43083–43089, https://doi.org/10.1021/acsami.0c12046.
[36] M.J. Inanlu, J. Farhadi, E. Ansari, S. Charkas, V. Bazargan, Effect of surfactant concentration on the evaporation-driven deposition of carbon nanotubes: from coffee-ring effect to strain sensing, RSC Adv. 12 (49) (2022) 31688–31698.
[37] Y. Liu, S. Yin, Z. Liu, H. Zhang, A machine learning framework for process optimization in aerosol jet 3D printing, Flex. Print. Electron. 8 (2) (2023) 025017.
[38] Y. Fang, H. Zou, S. Peng, G. Dong, M.M. Tentzeris, Full and In Situ Printing of Nanogenerators that Are Based on an Inherently Viscous Piezoelectric Polymer: An Effort to Minimize "Coffee Ring Effect" and Nonprinting Operations, ACS Appl. Electron. Mater. 5 (8) (2023) 4157–4167, https://doi.org/10.1021/acsaelm.3c00428.
[39] M. Zeng, H. Xie, M. Saeidi-Javash, A.N.M. Tanvir, Y. Du, J. Chen, M.G. Kanatzidis, Y. Zhang, Scalable nanomanufacturing of chalcogenide inks: a case study on thermoelectric V–VI nanoplates, J. Mater. Chem. A 9 (39) (2021) 22555–22562.
[40] D.B. Suits, A. Mason, L. Chan, Spline functions fitted by standard regression methods, Rev. Econ. Stat. (1978) 132–139.
[41] R.L. Eubank, Nonparametric Regression and Spline Smoothing, CRC Press, 1999.
[42] L.C. Marsh, D.R. Cormier, Spline Regression Models, Sage, 2001.
[43] M. Choël, K. Deboudt, J. Osán, P. Flament, R. Van Grieken, Quantitative Determination of Low-Z Elements in Single Atmospheric Particles on Boron Substrates by Automated Scanning Electron Microscopy−Energy-Dispersive X-ray Spectrometry, Anal. Chem. 77 (17) (2005) 5686–5692, https://doi.org/10.1021/ac050739x.
[44] S. Wang, G. Duan, Process parameter modeling for the fabrication of functionally graded materials via direct ink writing, Int. J. Adv. Manuf. Technol. 132 (7) (2024) 3415–3426.
[45] H. Zhang, J.P. Choi, S.K. Moon, T.H. Ngo, A hybrid multi-objective optimization of aerosol jet printing process via response surface methodology, Addit. Manuf. 33 (2020) 101096.
[46] R.R. Tafoya, A.W. Cook, B. Kaehr, J.R. Downing, M.C. Hersam, E.B. Secor, Real-time optical process monitoring for structure and property control of aerosol jet printed functional materials, Adv. Mater. Technol. 5 (12) (2020) 2000781.
[47] L. Gamba, M.E.A. Razzaq, S. Diaz-Arauzo, M.C. Hersam, X. Bai, E.B. Secor, Tailoring electrical properties in carbon nanomaterial patterns with multimaterial aerosol jet printing, ACS Appl. Mater. Interfaces 15 (49) (2023) 57525–57532.